RAA 2021 Vol. **21** No. **8**, 191(16pp) doi:10.1088/1674-4527/21/8/191

http://www.raa-journal.org *http://iopscience.iop.org/raa*

Research in Astronomy and Astrophysics

Reducing loss of significance in the computation of Earth-based two-way Doppler observables for small body missions

Wei-Tong Jin (金炜桐)[1,2], Fei Li (李斐)[1,3], Jian-Guo Yan (鄢建国)[1], Xuan Yang (杨轩)[1,2], Mao Ye (叶茂)[1], Wei-Feng Hao (郝卫峰)[3], Thomas Paul Andert[4] and Jean-Pierre Barriot[5]

[1] State Key Laboratory of Information Engineering in Surveying, Mapping and Remote Sensing, Wuhan University, Wuhan 430079, China; *fli@whu.edu.cn*; *jgyan@whu.edu.cn*

[2] State Key Laboratory of Satellite Navigation System and Equipment Technology, Shijiazhuang 050200, China; *jwt_whdx@whu.edu.cn*

[3] Chinese Antarctic Center of Surveying and Mapping, Wuhan University, Wuhan 430079, China

[4] Universität der Bundeswehr München, Neubiberg, Bayern, 85579, Germany

[5] University of French Polynesia, BP 6570, F-98702 Faa'a, Tahiti, French Polynesia

Received 2020 July 7; accepted 2021 March 19

Abstract Two-way Doppler measurement is a typical Earth-based radiometric technique for interplanetary spacecraft navigation and gravity science investigation. The most widely used model for the computation of two-way Doppler observables is Moyer's differenced-range Doppler (DRD) formula, which is based on a Schwarzschild approximation of the Solar-System space-time. However, the computation of range difference in DRD formula is sensitive to round-off errors due to approximate numbers defined by the norm IEEE754 in all PCs. This paper presented two updated models and their corresponding detailed instructions for the computation of the two-way Doppler observables so as to impair the effects of this type of numerical error. These two models were validated by two case studies related to the Rosetta mission—asteroid Lutetia flyby and comet 67P/Churyumov-Gerasimenko orbiting case. In these two cases, the numerical noise from the updated models can be reduced by two orders-of-magnitude in the computed two-way Doppler observables. The results showed an accuracy from better than 6×10^{-3} mm s^{-1} at 1 s counting time interval to better than 3×10^{-5} mm s^{-1} at 60 s counting time interval.

Key words: methods: numerical — space vehicles — planets and satellites: general

1 INTRODUCTION

Two significant tasks in interplanetary exploration conducted by robotic spacecraft are navigation and gravity science investigation. The core outputs of either task are based upon minimizing the residuals, computed as the differences between measured quantities and their computed values applying mathematical models in a least-squares sense (Zannoni & Tortora 2013), performed by spacecraft navigation and geophysical parameter estimation software (hereinafter referred to as navigation software). The emphasis is thus on mitigating the effects of noise in both measurements and corresponding computed observables, namely on improving the accuracy of both measurements and corresponding computed observables. Two-way Doppler, as an Earth-based radiometric tracking technique, is a typical type of measurement for interplanetary spacecraft navigation and gravity science investigation. The measurement accuracy becomes much higher thanks to the better performance of ground tracking systems, onboard Ultra-Stable Oscillators and multi-frequency observations so as to meet requirements for different missions.

The average measurement accuracy, scaled by the square root of the counting time (Pätzold et al. 2001), ranges from 0.1 to 0.02 mm s^{-1} at 60 s counting interval (Iess et al. 2012). For the Dawn mission, the accuracy is from 0.07 to 0.44 mm s^{-1} (Centinello et al. 2015). For the Mars Express (MEX) mission, the average accuracy is 0.051 mm s^{-1} at a 10 s counting interval (Pätzold et al. 2016b) whereas the value becomes around 0.05 mm s^{-1} at a 60 s counting interval (around $0.05\sqrt{60/10} \approx 0.12$ mm s^{-1} at a 10 s counting interval) for the Rosetta mission. However, this is not the end of the story. Observations at Ka band provide a significant improvement for Cassini two-way Doppler tracking. An accuracy of about 9×10^{-4} mm s^{-1} with a count time of 1000 s (around 0.009 mm s^{-1} at 10 s counting interval) was achieved during the gravitational wave experiment (GWE) that was part of the Cassini mission with additional help from solar opposition (Armstrong et al. 2003). Hence, corresponding computed observables are necessary to be obtained with a high accuracy, aiming at the exploitation of valuable assets.

Errors in the computed two-way Doppler observables are caused by incomplete mathematical models and numerical errors that occur in the computation performed by the navigation software relying on these models (Zannoni & Tortora 2013). A two-way Doppler model named "differenced-range Doppler" (DRD), developed by Moyer (2005), is based upon a Schwarzschild approximation of the Solar-System space-time and is most widely implemented in authoritative navigation software such as NASA/Jet Propulsion Laboratory (JPL), California Institute of Technology's Orbit Determination Program (ODP), and Mission-Analysis, Operations, and Navigation Toolkit Environment (MONTE), ESA's Advanced Modular Facility for Interplanetary Navigation (AMFIN) and NASA's Goddard Space Flight Center's GEODYN-II. The core of this model is calculating a simple differencing of two subsequent ranges (at the start and the end of counting time) between the Earth station and the spacecraft. For a distant probe at several AUs, the numerical accuracy of the range in the software compiled in double-precision mode is at the level of millimeters. This corresponds to using double-precision floating-point numbers (Iess et al. 2012; IEEE 2019), giving the numerical accuracy of 16 digits. This level is enough for the range of measurement accuracy. However, large errors will be induced by the simple differencing of two large ranges corresponding to loss of significance, not the range itself.

In general, there are two strategies for reducing the loss of significance in the two-way Doppler model. One is compiling the navigation program using the floating-point representation in a higher precision, such as quadruple-precision representation. However, it increases both the complexity of the source code and the execution time of the program. Moreover, the published ephemerides of the celestial bodies are stored in a double-precision-mode and we have to consider the compatibility between a subset of procedures processing the ephemerides in double-precision and other subroutines recompiled in quadruple precision. This strategy is thus not widely adopted in these software packages.

The other method is reducing the loss of significance from a mathematical point of view, i.e. reconstructing the differencing of two large numbers by applying mathematical models. ODP and AMFIN implement an older formula, based upon a truncated Taylor series, called the integrated Doppler (ID) formulation (Zannoni & Tortora 2013). As described in detail in Moyer (1971), the computation of two-way Doppler observables is obtained by expanding the frequency shift into a Taylor series, with coefficients evaluated at the midpoint of the count interval, and integrating term by term. However, this formulation was then replaced by DRD formulation in lots of navigation software such as the current version of ODP and MONTE (Zannoni & Tortora 2013) due to limits on the counting time. GEODYN-II refined DRD formulation based upon the fact that the geometrical spacecraft-ground range difference can be expanded into a multidimensional Taylor series. The refined DRD formula was described in Rowlands et al. (2015), where the impact on the accuracy of Mars spacecraft navigation was also discussed. However, we found another crucial fact, which was not considered in Rowlands et al. (2015), that this formulation would be ineffective if the center of integration is the Sun. This is because the simple differencing of two subsequent spacecraft positions in J2000 frame is utilized in this model. This will also induce the loss of significance for the spacecraft far away from the Sun. Moreover, this formula is not applicable when the ephemeris of the central body, such as a small body, is not in the form of Chebyshev. Tommei et al. (2010) proposed a 7-node Gaussian quadrature formula that is incorporated into the computation of the averaged value of range rate over large count times. However, this detailed formula, containing the development of a new time coordinate Mercury Dynamic Time (TDM) for testing general relativity in the BepiColombo mission, is a complicated complement for regular two-way Doppler models. For these reasons, more detailed formulas of the two-way Doppler observables for reducing loss of significance are necessary to be studied and developed.

This paper proposes two updated models of computed two-way Doppler observables for reducing loss of significance, considering different count times and centers of integration. In Section 2, both updated models and their corresponding detailed instructions are introduced, as well as a basic description of DRD model. The validation and limits of both models are analyzed in Section 3 by two case studies related to the Rosetta mission—asteroid Lutetia flyby and comet 67P/Churyumov-Gerasimenko (hereinafter referred to as comet 67P) orbiting case. At last, Section 4 draws the conclusions.

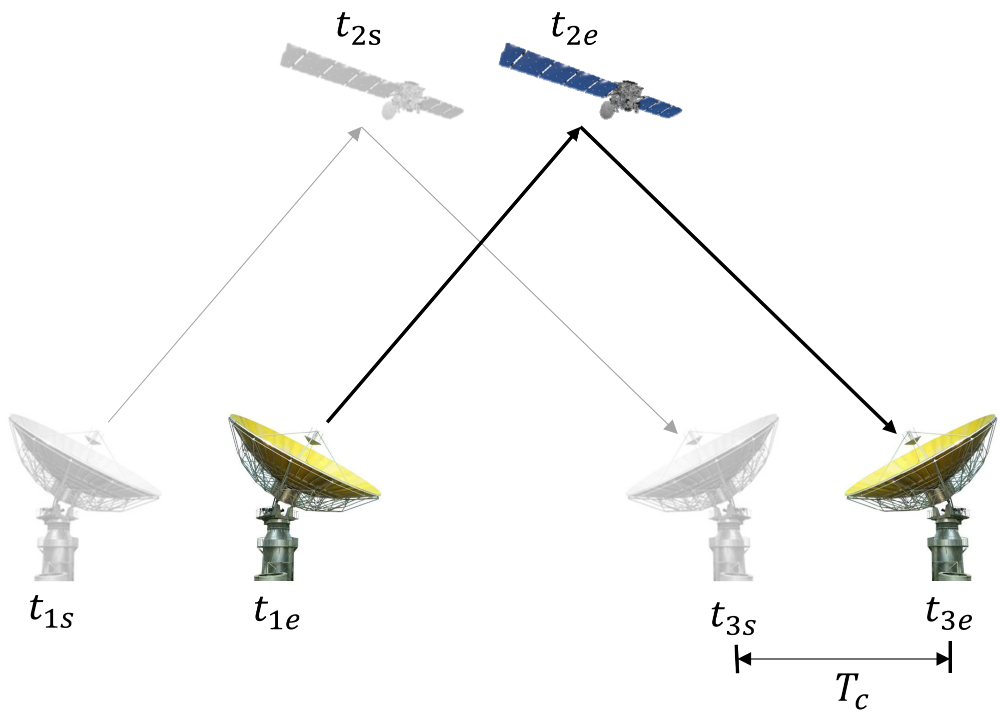

Fig. 1 Schematic diagram of Doppler measurements in the two-way mode.

2 UPDATED MODELS OF COMPUTING TWO-WAY DOPPLER OBSERVABLES

2.1 Traditional Moyer's Two-way Doppler Model (DRD model)

The measured quantity of Doppler tracking is the relative velocity between a spacecraft and a ground station. In the two-way mode, illustrated by Figure 1, the ground station transmits an uplink radio signal at the epoch t_{1s} and the spacecraft sends back a frequency-shifted replica of the received signal at the epoch t_{2s}. The same ground station receives the downlink radio signal at the epoch t_{3s}. Likewise, the ground station transmits an uplink radio signal at the epoch t_{1e} and the spacecraft sends back a frequency-shifted replica of the received signal at the epoch t_{2e}. The same ground station receives the downlink radio signal at the epoch t_{3e}. $t_{3e} - t_{3s}$ is the counting interval T_c. The data time tag is the midpoint of the counting interval.

Here we discuss merely the formulation with a constant uplink frequency, i.e. un-ramped DRD model, expressed as Moyer (2005)

$$C_{\text{unramped}} = \frac{1}{2}\left(\frac{r_n^u(t_{3e}) - r_n^u(t_{3s})}{T_c} + \frac{r_n^d(t_{3e}) - r_n^d(t_{3s})}{T_c}\right) + \frac{1}{2}\left(\frac{r_s^u(t_{3e}) - r_s^u(t_{3s})}{T_c} + \frac{r_s^d(t_{3e}) - r_s^d(t_{3s})}{T_c}\right) \tag{1}$$

where C_{unramped} is the computed value of two-way Doppler observables, $r_n^u(t_{3e})$ is the Euclidean range between the ground station at time t_{1e} and the spacecraft at time t_{2e}, $r_n^u(t_{3s})$ is the Euclidean range between the ground station at time t_{1s} and the spacecraft at time t_{2s}, $r_n^d(t_{3e})$ is the Euclidean range between the ground station at time t_{3e} and the spacecraft at time t_{2e}, $r_n^d(t_{3s})$ is the Euclidean range between the ground station at time t_{3s} and the spacecraft at time t_{2s}, $r_s^u(t_{3e})$ is the sum of range of second-order terms (relativistic light-time delays, time-scale transformations, electronic delays and transmission media delays) in the uplink from t_{1e} to t_{2e}, $r_s^u(t_{3s})$ is the sum of range of second-order terms in the uplink from t_{1s} to t_{2s}, $r_s^d(t_{3e})$ is the sum of range of second-order terms in the downlink from t_{3e} to t_{2e} and $r_s^d(t_{3s})$ is the sum of range of second-order terms in the downlink from t_{3s} to t_{2s}.

The computations of $r_n^u(t_{3e})$, $r_n^u(t_{3s})$, $r_n^d(t_{3e})$ and $r_n^d(t_{3s})$ follow an iterative step of uplink and downlink light-time computation. Here the emphasis is on the reason why Equation (1) is sensitive to numerical errors instead of on the computation of these eight ranges, which is described by Moyer (2005) in detail.

The source codes of most navigation software are compiled in double-precision representation, following the IEEE754 standard (IEEE 2019). For a double precision number with 64 bit word, only 52 bits are used for the mantissa and the resulting maximum relative error is about 1.1×10^{-16}, corresponding to around 0.15 mm range error at 10 AU (Iess et al. 2012). Moreover, the

Table 1 Simulation Setup for the Validation and Analysis of UTD Model

Setups related to spacecraft	
Central body	Sun
N-body perturbation	JPL DE430 Ephemeris (eight planets, Earth's Moon, Pluto), three big asteroids (Folkner et al. 2014)
Perturbation from Lutetia	GM = 0.1134 km^3 s^{-2} (Pätzold et al. 2011)
Relativistic Perturbation	Point mass of the Sun (Moyer 2005)
Solar radiation pressure	Canon ball model (Montenbruck & Gill 2012)
Setups related to ground station	
Tracking station	DSS 63
Counting interval	1 s, 5 s and 10 s
Tracking gap	without tracking gap
Tracking span	from 4 hr before closest approach to 6 hr after closest approach

value of Earth-spacecraft Euclidean ranges at t_{3e} and t_{3s} is large and nearly equal for interplanetary missions. The characteristics of IEEE754 floating-point algorithms reveal that their simple differencing $r_n^u(t_{3e}) - r_n^u(t_{3s})$ and $r_n^d(t_{3e}) - r_n^d(t_{3s})$ will introduce much loss of significant digits. $r_s^u(t_{3e}) - r_s^u(t_{3s})$ and $r_s^d(t_{3e}) - r_s^d(t_{3s})$ can be by contrast computed accurately compared to the present level of noise in the measurements. We will not discuss in this paper this type of error since Zannoni & Tortora (2013) analyzed the statistical character of this numerical noise and presented a mathematical model for the expected numerical errors in the two-way Doppler observables computed with the DRD model. We will step up efforts to develop updated two-way Doppler mathematical models to mitigate as much as possible the effects of this type of numerical noise.

2.2 GEODYN-II's Interplanetary Doppler Model (GID model)

The GID model can be considered as an improved version of the DRD model since $r_n^u(t_{3e}) - r_n^u(t_{3s})$ and $r_n^d(t_{3e}) - r_n^d(t_{3s})$ are computed to a high numerical precision whereas the computation of $r_s^d(t_{3e}) - r_s^d(t_{3s})$ and $r_s^d(t_{3e}) - r_s^d(t_{3s})$ follows the DRD formulation. In the GID model, $r_n^u(t_{3e}) - r_n^u(t_{3s})$ and $r_n^d(t_{3e}) - r_n^d(t_{3s})$ are respectively expanded into a multidimensional Taylor series at t_{3s}. Here we give the formulas of these two differenced-ranges as follows.

$$\begin{aligned} r_n^d(t_{3e}) - r_n^d(t_{3s}) = {} & f_d^{(1)}(0,0,0)\|\mathbf{D}\| \\ & + \frac{1}{2} f_d^{(2)}(0,0,0)\|\mathbf{D}\|^2 \\ & + \frac{1}{6} f_d^{(3)}(0,0,0)\|\mathbf{D}\|^3 + O\left(\|\mathbf{D}\|^3\right) \end{aligned} \quad (2)$$

where $\mathbf{D}$ is the downlink change vector and f_d is the representation of $r_n^d(t_{3e})$ as a function of downlink change vector. Here $O(\|\mathbf{D}\|^3)$ is neglected and $f_d^{(1)}(0,0,0)$, $f_d^{(2)}(0,0,0)$ and $f_d^{(3)}(0,0,0)$ are computed as:

$$f_d^{(1)}(0,0,0) = \frac{\mathbf{n_d R_d}}{r_n^d(t_{3s})} \quad (3)$$

$$f_d^{(2)}(0,0,0) = \frac{r_n^d(t_{3s}) - \frac{1}{r_n^d(t_{3s})}(\mathbf{n_d R_d})}{\left(r_n^d(t_{3s})\right)^2} \quad (4)$$

$$f_d^{(3)}(0,0,0) = \frac{r_n^d(t_{3s})(\mathbf{n_d R_d})(-1-2s_d) + \frac{3}{r_n^d(t_{3s})}(\mathbf{n_d R_d})^3}{\left(r_n^d(t_{3s})\right)^4} \quad (5)$$

where $\mathbf{n_d}$ is the unit vector of $\mathbf{D}$, $\mathbf{R_d}$ is the barycentric position vector from the spacecraft at time t_{2s} to the ground station at time t_{3s}, and s_d is the sum of three components of $\mathbf{n_d}$, $\mathbf{R_d}$ and D which can be computed as

$$\mathbf{R_d} = \mathbf{X_E}(t_{3s}) + \mathbf{X}_{\text{GS}}(t_{3s}) - \mathbf{X_C}(t_{2s}) - \mathbf{X}_{\text{SC}}(t_{2s}) \quad (6)$$

where $\mathbf{X_E}(t_{3s})$ is the barycentric position of the Earth at time t_{3s}, $\mathbf{X}_{\text{GS}}(t_{3s})$ is the barycentric position of the ground station as seen from the Earth at time t_{3s}, $\mathbf{X_C}(t_{2s})$ is the barycentric position of the central body at time t_{2s} and $\mathbf{X}_{\text{SC}}(t_{2s})$ is the barycentric position of the spacecraft as seen from the central body at time t_{2s}.

$$\text{D} = \mathbf{X_E^d} + \mathbf{X}_{\text{GS}}^{\mathbf{d}} - \mathbf{X_C} - \mathbf{X}_{\text{SC}} \quad (7)$$

where $\mathbf{X_E^d}$ is the barycentric position difference vector from the solar system barycenter to the Earth at times t_{3e} and t_{3s}, $\mathbf{X}_{\text{GS}}^{\mathbf{d}}$ is the barycentric position difference vector from the Earth to the ground station at times t_{3e} and t_{3s}, $\mathbf{X_C}$ is the barycentric position difference vector from the solar system barycenter to the central body at times t_{2e} and t_{2s}, and X_{SC} is the barycentric position difference vector from the central body to the spacecraft at times t_{2e} and t_{2s}. Here $\mathbf{X}_{\text{GS}}^{\mathbf{d}}$ and $\mathbf{X}_{\text{SC}}$ are computed directly as:

$$\mathbf{X}_{\text{GS}}^{\mathbf{d}} = \mathbf{X}_{\text{GS}}(t_{3e}) - \mathbf{X}_{\text{GS}}(t_{3s}) \quad (8)$$

$$\mathbf{X}_{\text{SC}} = \mathbf{X}_{\text{SC}}(t_{2e}) - \mathbf{X}_{\text{SC}}(t_{2s}) \quad (9)$$

where $\mathbf{X}_{\text{GS}}(t_{3e})$ is the barycentric position of the ground station as seen from the Earth at times t_{3e}, and $\mathbf{X}_{\text{SC}}(t_{2e})$ is

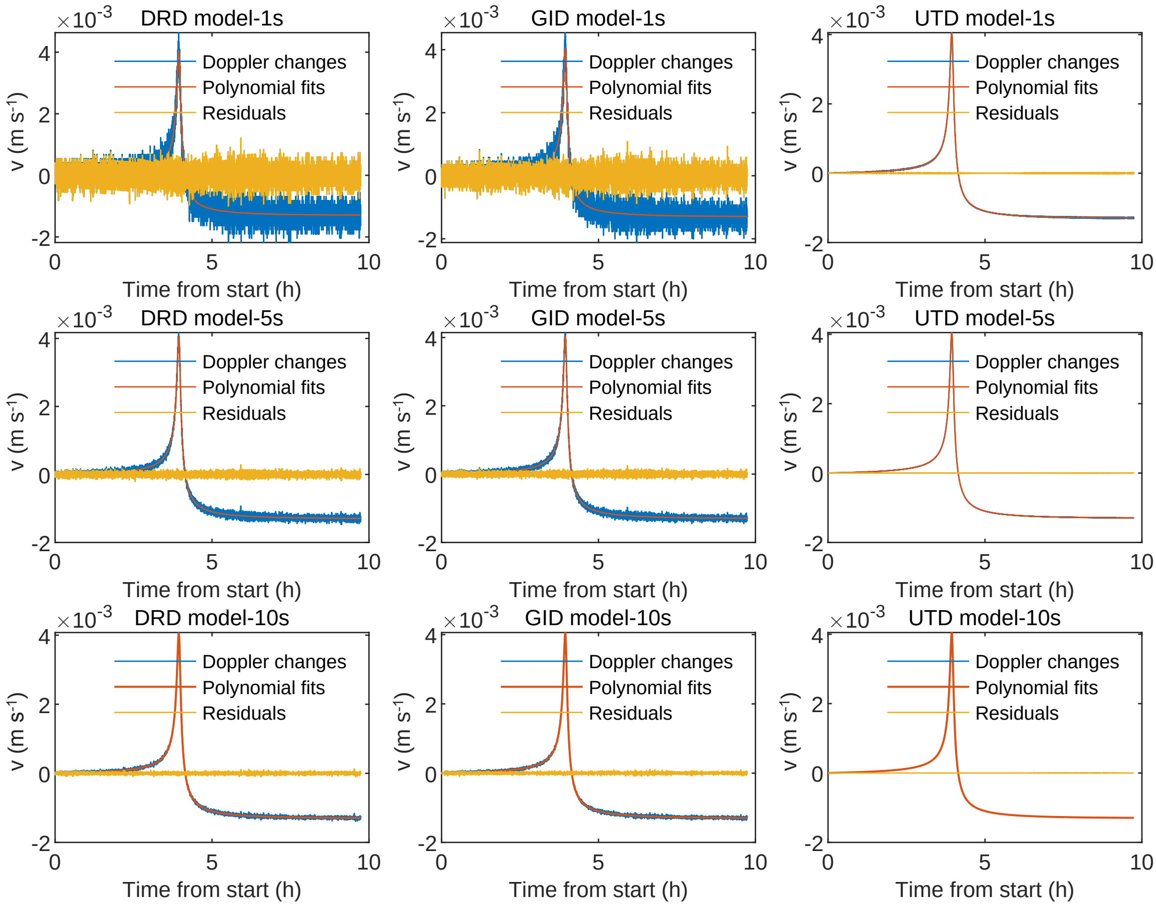

Fig. 2 Changes in the simulated two-way Doppler observables ($\mathrm{m\,s^{-1}}$) due to the mass of Lutetia at 1 s, 5 s and 10 s counting time.

the barycentric position of the spacecraft as seen from the central body at time t_{2e}.

It is necessary to compute $\mathbf{X_C}$ and $\mathbf{X_E^d}$ in Equation (7) as:

$$\mathbf{X_C} = \sum_{k=0}^{NC-1} C_{k\ 3\times1}^{C}\left(\tau_{2s}\right) P_k^C \tag{10}$$

$$\mathbf{X_E^d} = \sum_{k=0}^{12}\left(C_{k\ 3\times1}^{\mathrm{EB}}\left(\tau_{3s}^{\mathrm{EB}}\right) P_k^{\mathrm{EBd}} - \frac{C_{k\ 3\times1}^{M}\left(\tau_{3s}^{M}\right)}{1+\frac{\mu_E}{\mu_M}} P_k^{\mathrm{Md}}\right) \tag{11}$$

where τ_{2s} is time t_{2s} in the domain of Chebyshev for the central body, τ_{3s}^{EB} is time t_{3s} in the domain of Chebyshev for the Earth-Moon barycenter, τ_{3s}^{M} is time t_{3s} in the domain of Chebyshev for the Earth's Moon, NC is the order of the Chebyshev polynomial for the central body, $C_{k\ 3\times1}^{C}\left(\tau_{2s}\right)$ is Chebyshev coefficients at τ_{2s} for the central body, $C_{k\ 3\times1}^{\mathrm{EB}}\left(\tau_{3s}^{\mathrm{EB}}\right)$ is Chebyshev coefficients at τ_{3s}^{EB} for the Earth-Moon barycenter, $C_{k\ 3\times1}^{M}\left(\tau_{3s}^{M}\right)$ is Chebyshev coefficients at τ_{3s}^{M} for the Earth's Moon, P_k^C is Chebyshev differencing polynomials for the central body, k=0,1,2…NC, P_k^{EBd} is Chebyshev differencing polynomials of the Earth-Moon barycenter for the downlink signal, k=0,1,2…,12, P_k^{Md} is Chebyshev differencing polynomials of the Earth's Moon for the downlink signal, k=0,1,2…,12, μ_E and μ_M are the standard gravitational parameter of the Earth and Earth's Moon, respectively. Here τ_{2s}, τ_{3s}^{EB} and τ_{3s}^{M} are all computed utilizing official subroutines provided by JPL; $C_{k\ 3\times1}^{C}\left(\tau_{2s}\right)$, $C_{k\ 3\times1}^{\mathrm{EB}}\left(\tau_{3s}^{\mathrm{EB}}\right)$ and $C_{k\ 3\times1}^{M}\left(\tau_{3s}^{M}\right)$ are all obtained from JPL celestial ephemeris.

P_k^c in Equation (10) is computed applying the following recurrence relationship

$$P_0^C = 0 \tag{12}$$

$$P_1^C = \tau_{2e} - \tau_{2s} \tag{13}$$

$$\cdots$$

$$P_k^C = 2\tau_{2e}P_{k-1}^C + 2\left(\tau_{2e} - \tau_{2s}\right)P_k^C\left(\tau_{2s}\right) - P_{k-2}^C \tag{14}$$

and $P_k(\tau_{2s})$ is the Chebyshev polynomial, computed using the recurrence relationship described in Montenbruck & Gill (2012). Likewise, P_k^{EBd} in Equation (11) is obtained by replacing C with EBd, τ_{2e} with τ_{3e}^{EB} and τ_{2s} with τ_{3s}^{EB}. P_k^{Md} is obtained by replacing C with Md, τ_{2e} with τ_{3e}^{M} and τ_{2s} with τ_{3s}^{M}.

Table 2 The Mean Value (MV) and Standard Deviation (STD) of the Differences between Simulated Doppler Changes and Their Polynomial Fits Using Different Models at Different Count Times

	1s-count time		5s-count time		10s-count time	
$\mathrm{m\,s^{-1}}$	MV	STD	MV	STD	MV	STD
DRD model	1.3509e-07	1.8424e-04	1.3495e-07	5.6168e-05	1.3742e-07	2.9579e-05
GID model	1.3399e-07	1.2432e-04	1.3397e-07	4.9070e-05	1.3802e-07	2.6043e-05
UTD model	1.2094e-07	5.5251e-06	1.2094e-07	1.1164e-06	1.2093e-07	5.7720e-07

$r_n^u(t_{3e}) - r_n^u(t_{3s})$ can be computed in a similar way as

$$r_n^u(t_{3e}) - r_n^u(t_{3s}) = f_u^{(1)}(0,0,0)\,\|\mathbf{U}\| + \frac{1}{2} f_u^{(2)}(0,0,0)\,\|\mathbf{U}\|^2 + \frac{1}{6} f_u^{(3)}(0,0,0)\,\|\mathbf{U}\|^3 + O\left(\|\mathbf{U}\|^3\right) \quad (15)$$

where f_u is the representation of $r_n^u(t_{3e})$ as the function of uplink change vector and $\mathbf{U}$ is uplink change vector. Here $O(\|\mathbf{U}\|^3)$ is neglected and $f_u^{(1)}(0,0,0)$, $f_u^{(2)}(0,0,0)$ and $f_u^{(3)}(0,0,0)$ are computed as

$$f_u^{(1)}(0,0,0) = \frac{\mathbf{n_u R_u}}{r_n^u(t_{3s})} \quad (16)$$

$$f_u^{(2)}(0,0,0) = \frac{r_n^u(t_{3s}) - \frac{1}{r_n^u(t_{3s})}(\mathbf{n_u R_u})}{\left(r_n^u(t_{3s})\right)^2} \quad (17)$$

$$f_u^{(3)}(0,0,0) = \frac{r_n^u(t_{3s})(\mathbf{n_u R_u})(-1-2s_u) + \frac{3}{r_n^u(t_{3s})}(\mathbf{n_u R_u})^3}{\left(r_n^u(t_{3s})\right)^4} \quad (18)$$

where $\mathbf{n_u}$ is the unit vector of $\mathbf{U}$, $\mathbf{R_u}$ is the barycentric position vector from the spacecraft at time t_{2s} to the ground station at time t_{1s} and s_u is the sum of three components of $\mathbf{n_u}$, $\mathbf{R_u}$ and $\mathbf{U}$ which can be computed as

$$\mathbf{R_u} = \mathbf{X_E}(t_{1s}) + \mathbf{X}_{\mathrm{GS}}(t_{1s}) - \mathbf{X_C}(t_{2s}) - \mathbf{X}_{\mathrm{SC}}(t_{2s}) \quad (19)$$

where $\mathbf{X_E}(t_{1s})$ is the barycentric position of the Earth at time t_{1s} and $\mathbf{X}_{\mathrm{GS}}(t_{1s})$ is the barycentric position of the ground station as seen from the Earth at time t_{1s}.

$$\mathrm{U} = \mathbf{X_E^u} + \mathbf{X_{GS}^u} - \mathbf{X_C} - \mathbf{X}_{\mathrm{SC}} \quad (20)$$

where $\mathbf{X_E^u}$ is the barycentric position difference vector from the solar system barycenter to the Earth at time t_{1e} and t_{1s}, and $\mathbf{X_{GS}^u}$ is the barycentric position difference vector from the Earth to the ground station at time t_{1e} and t_{1s}. Here $\mathbf{X_{GS}^u}$ is computed directly as

$$\mathbf{X_{GS}^u} = \mathbf{X}_{\mathrm{GS}}(t_{1e}) - \mathbf{X}_{\mathrm{GS}}(t_{1s}) \quad (21)$$

where $\mathbf{X}_{\mathrm{GS}}(t_{1e})$ is the barycentric position of the ground station as seen from the Earth at time t_{1e}, and where $\mathbf{X}_{\mathrm{GS}}(t_{1s})$ is the barycentric position of the ground station as seen from the Earth at time t_{1s}.

$\mathbf{X_E^u}$ in Equation (20) is necessary to be computed as

$$\mathbf{X_E^u} = \sum_{k=0}^{12}\left(C_{k\ 3\times1}^{\mathrm{EB}}\left(\tau_{1s}^{\mathrm{EB}}\right)P_k^{\mathrm{EBu}} - \frac{C_{k\ 3\times1}^{M}\left(\tau_{1s}^{M}\right)}{1+\frac{\mu_E}{\mu_M}}P_k^{\mathrm{Mu}}\right) \quad (22)$$

where τ_{1s}^{EB} is time t_{1s} in the domain of Chebyshev for the Earth-Moon barycenter, τ_{1s}^{M} is time t_{1s} in the domain of Chebyshev for the Earth's Moon, $C_{k\ 3\times1}^{\mathrm{EB}}\left(\tau_{1s}^{\mathrm{EB}}\right)$ is Chebyshev coefficients at τ_{1s}^{EB} for the Earth-Moon barycenter and $C_{k\ 3\times1}^{M}\left(\tau_{1s}^{M}\right)$ is Chebyshev coefficients at τ_{1s}^{M} for the Earth's Moon. Here τ_{1s}^{EB} and τ_{1s}^{M} are computed utilizing official subroutines provided by JPL; $C_{k\ 3\times1}^{\mathrm{EB}}\left(\tau_{1s}^{\mathrm{EB}}\right)$ and $C_{k\ 3\times1}^{M}\left(\tau_{1s}^{M}\right)$ are obtained from JPL celestial ephemeris. P_k^{EBu} is computed via the same formulas with P_k^{EBd} by replacing *EBd* with *EBu*, τ_{3e}^{EB} with τ_{1e}^{EB} and τ_{3s}^{EB} with τ_{1s}^{EB}. P_k^{Mu} is computed applying the same formulas with P_k^{Md} by replacing *Md* with *Mu*, τ_{3e}^{M} with τ_{1e}^{M} and τ_{3s}^{M} with τ_{1s}^{M}.

2.3 Our Updated Doppler Model Based on Taylor Series (UTD model)

The UTD model, considering the case when the central body of the spacecraft is the Sun, is in a sense a supplement to the GID model. The supplement contains the following three aspects of improvement.

1) The formulas of $f_u^{(3)}(0,0,0)$ and $f_d^{(3)}(0,0,0)$ are updated since Equations (3) and Equation (18) are considered not correct.
2) The formulas of $\mathbf{X_E^u}$, $\mathbf{X_E^d}$ and $\mathbf{X_C}$ are updated since the case is considered that corresponding time tags related to the start and the end of Doppler counting interval fall into two separate JPL time blocks.
3) When the central body of the spacecraft is the Sun, it is necessary to update the formula $\mathbf{X}_{\mathrm{SC}}$ into a new version since the direct computation of Equation (9) would introduce large numerical errors.

In the UTD model, $f_d^{(3)}(0,0,0)$ and $f_u^{(3)}(0,0,0)$ are expressed as:

$$f_d^{(3)}(0,0,0) = \frac{-3r_n^d(t_{3s})(\mathbf{n_d R_d}) + \frac{3}{r_n^d(t_{3s})}(\mathbf{n_d R_d})^3}{\left(r_n^d(t_{3s})\right)^4} \quad (23)$$

Table 3 Simulation Setup for the Validation and Analysis of UID Model

Setups related to spacecraft	
Central body	Comet 67P 3× 3 gravity field, where C_{11} is 7.38e-5
N-body perturbation	JPL DE430 Ephemeris (eight planets, Earth's Moon, Pluto), three big asteroids (Folkner et al. 2014)
Relativistic Perturbation	Point mass of the Sun (Moyer 2005)
Solar radiation pressure	Canon ball model (Montenbruck & Gill 2012)
Outgassing model	As described in Godard et al. (2015)
Setups related to ground station	
Tracking station	DSS 34
Counting interval	10 s, 30 s and 60 s
Tracking gap	without tracking gap
Tracking span	2016-05-25T09:48:53.949 - 2016-05-25T13:27:49.949

$$f_u^{(3)}(0,0,0) = \frac{-3r_n^u(t_{3s})(\mathbf{n_u R_u}) + \frac{3}{r_n^u(t_{3s})}(\mathbf{n_u R_u})^3}{(r_n^u(t_{3s}))^4}. \tag{24}$$

Moreover, $\mathbf{X_C}$, $\mathbf{X_E^d}$ and $\mathbf{X_E^u}$ can be computed in the UTD model as

$$\mathbf{X_C} = \sum_{k=0}^{NC-1}\left[C^C_{k\ 3\times1}(\tau_{2s})P^C_k + C^C_{k_{3\times1}}P^C_k(\tau_{2e})\right] \tag{25}$$

$$\mathbf{\Delta X_E^d} = \sum_{k=0}^{12}\left[\begin{array}{l}\left(C^{EB}_{k\ 3\times1}(\tau^{EB}_{3s})\Delta P^{EBd}_k - \frac{C^M_{k\ 3\times1}(\tau^M_{3s})}{1+\frac{\mu_E}{\mu_M}}\Delta P^{Md}_k\right) + \\ \left(\Delta C^{EBd}_{k\ 3\times1}P^{EB}_k(\tau^{EB}_{3e}) - \frac{\Delta C^{Md}_{k\ 3\times1}}{1+\frac{\mu_E}{\mu_M}}P^M_k(\tau^M_{3e})\right)\end{array}\right] \tag{26}$$

$$\mathbf{\Delta X_E^u} = \sum_{k=0}^{12}\left[\begin{array}{l}\left(C^{EB}_{k\ 3\times1}(\tau^{EB}_{1s})\Delta P^{EBu}_k - \frac{C^M_{k\ 3\times1}(\tau^M_{1s})}{1+\frac{\mu_E}{\mu_M}}\Delta P^{Mu}_k\right) + \\ \left(\Delta C^{EBu}_{k\ 3\times1}P^{EB}_k(\tau^{EB}_{1e}) - \frac{\Delta C^{Mu}_{k\ 3\times1}}{1+\frac{\mu_E}{\mu_M}}P^M_k(\tau^M_{1e})\right)\end{array}\right] \tag{27}$$

where

$$C^C_{k_{3\times1}} = C^C_{k\ 3\times1}(\tau_{2e}) - C^C_{k\ 3\times1}(\tau_{2s}) \tag{28}$$

$$C^{\rm EBd}_{k\ \ 3\times1} = C^{\rm EB}_{k\ 3\times1}(\tau^{\rm EB}_{3e}) - C^{\rm EB}_{k\ 3\times1}(\tau^{\rm EB}_{3s}) \tag{29}$$

$$C^{\rm Md}_{k\ \ 3\times1} = C^M_{k\ 3\times1}(\tau^M_{3e}) - C^M_{k\ 3\times1}(\tau^M_{3s}) \tag{30}$$

$$C^{\rm EBu}_{k\ \ 3\times1} = C^{\rm EB}_{k\ 3\times1}(\tau^{\rm EB}_{1e}) - C^{\rm EB}_{k\ 3\times1}(\tau^{\rm EB}_{1s}) \tag{31}$$

$$C^{\rm Mu}_{k\ \ 3\times1} = C^M_{k\ 3\times1}(\tau^M_{1e}) - C^M_{k\ 3\times1}(\tau^M_{1s}). \tag{32}$$

Here τ_{2e} is time t_{2e} in the domain of Chebyshev for the central body, $\tau^{\rm EB}_{3e}$ is time t_{3e} in the domain of Chebyshev for the Earth-Moon barycenter, τ^M_{3e} is time t_{3e} in the domain of Chebyshev for the Earth's Moon, $\tau^{\rm EB}_{1e}$ is time t_{1e} in the domain of Chebyshev for the Earth-Moon barycenter, τ^M_{1e} is time t_{1e} in the domain of Chebyshev for the Earth's Moon, $C^C_{k\ 3\times1}(\tau_{2e})$ is Chebyshev coefficients at τ_{2e} for the central body, $C^{\rm EB}_{k\ 3\times1}(\tau^{\rm EB}_{3e})$ is Chebyshev coefficients at $\tau^{\rm EB}_{3e}$ for the Earth-Moon barycenter, $C^M_{k\ 3\times1}(\tau^M_{3e})$ is Chebyshev coefficients at τ^M_{3e} for the Earth's Moon, $C^{\rm EB}_{k\ 3\times1}(\tau^{\rm EB}_{1e})$ is Chebyshev coefficients at $\tau^{\rm EB}_{1e}$ for the Earth-Moon barycenter and $C^M_{k\ 3\times1}(\tau^M_{1e})$ is Chebyshev coefficients at τ^M_{1e} for the Earth's Moon. If corresponding time tags, related to the start and end of Doppler counting interval, fall within the same JPL time block, the second term in Equations (25)–(27) will vanish since values of Equations (28)–(32) are all zero.

When the central body of the spacecraft is the Sun, $\mathbf{X}_{\rm SC}(t_{2s})$ and $\mathbf{X}_{\rm SC}(t_{2e})$ are in general large and nearly equal. Here we give the following detailed derivation of the formula for $\mathbf{X}_{\rm SC}$.

The spacecraft orbit around the central body is obtained by solving the following differential equation numerically.

$$\frac{d\mathbf{X}_{\rm SC}}{dt} = h(t, \mathbf{X}_{\rm SC}) \tag{33}$$

where h is the differential equation for spacecraft trajectories.

The spacecraft state vector at time t_{2e} can be represented using the s-order Runge-Kutta method (Montenbruck & Gill 2012).

$$\mathbf{X}_{\rm SC}(t_{2e}) = \mathbf{X}_{\rm SC}(t_{2s}) + (t_{2e} - t_{2s})\sum_{i=1}^{s} b_i k_{i_{6\times1}} \tag{34}$$

where

$$k_{i_{6\times1}} = h\left(t_{2s} + c_i(t_{2e} - t_{2s}), \mathbf{X}_{\rm SC}(t_{2s}) + (t_{2e} - t_{2s})\sum_{j=1}^{s} a_{\rm ij}k_{i_{6\times1}}\right). \tag{35}$$

Here $a_{\rm ij}$, b_i and c_i are coefficients for the s-order Runge-Kutta method. Thus,

$$\mathbf{X}_{\mathbf{SC}_{6\times1}}(t_{2e}) = (t_{2e} - t_{2s})\sum_{i=1}^{s} b_i k_{i_{6\times1}}. \tag{36}$$

Finally, the complete instruction for the UTD model is given by performing the following steps.

1) Obtain light time solution of downlink and uplink radio signals as described in Moyer (2005), starting

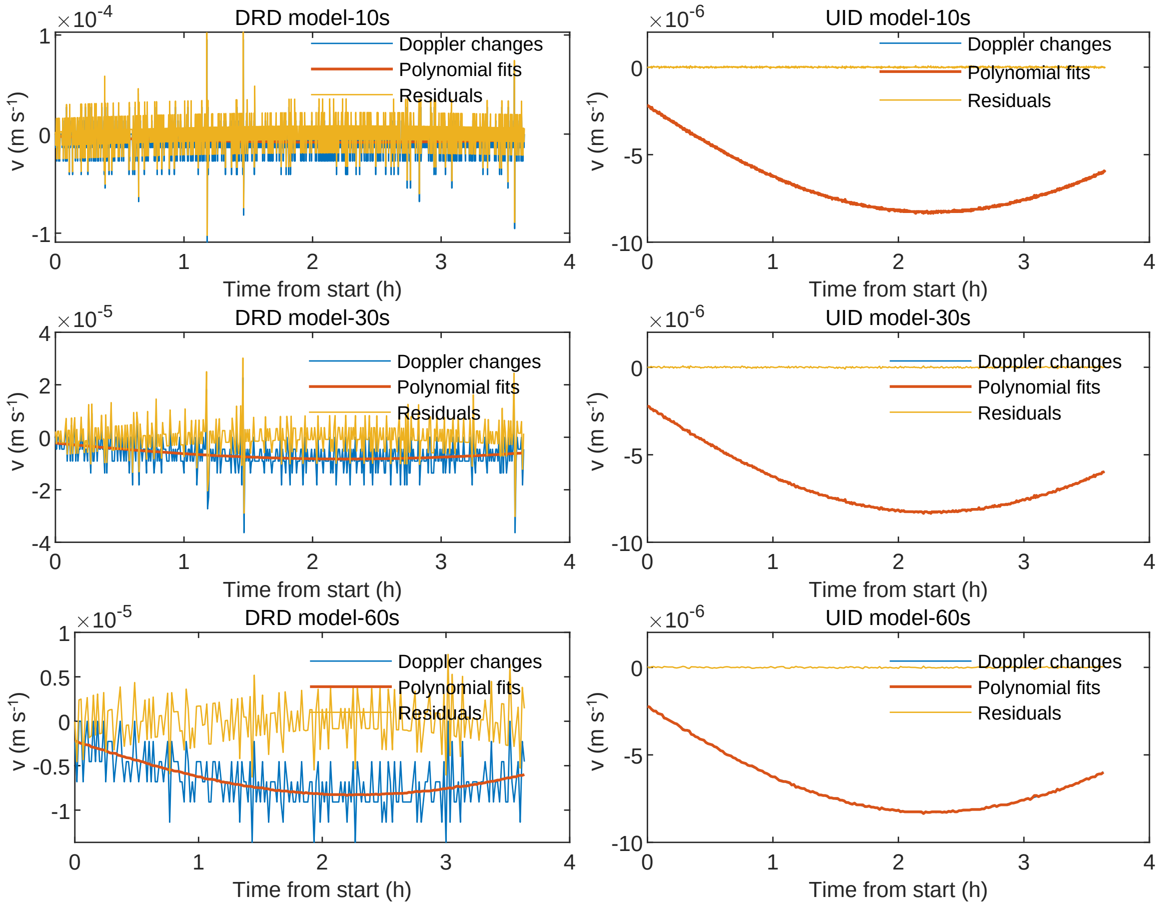

Fig. 3 Changes in simulated two-way Doppler observables due to C_{11} harmonic coefficient of comet 67P's gravity field at 10 s, 30 s and 60 s counting time, from top to bottom respectively.

Table 4 The Mean Value (MV) and Standard Deviation (STD) of the Differences between Simulated Doppler Changes and Their Polynomial Fits Using Different Models at Different Count Times

	10 s-count time		30 s-count time		60 s-count time	
m s^{-1}	MV	STD	MV	STD	MV	STD
DRD model	2.2649e-09	1.7385e-05	9.7848e-09	6.0363e-06	–4.8964e-09	2.4454e-06
UID model	5.4480e-10	2.6865e-08	4.7516e-10	2.8222e-08	–1.6411e-09	2.9575e-08

from t_{3e}. Then t_{2e} is computed iteratively, and, using this information t_{1e} is computed. Meanwhile, $\mathbf{X_E}(t_{3e})$, $\mathbf{X}_{\mathrm{GS}}(t_{3e})$, $\mathbf{X_C}(t_{2e})$, $\mathbf{X}_{\mathrm{SC}}(t_{2e})$, $\mathbf{X_E}(t_{1e})$ and $\mathbf{X}_{\mathrm{GS}}(t_{1e})$ are obtained. Moreover, we need to store values of τ_{3e}^{EB}, $C_{k\ 3\times1}^{\mathrm{EB}}(\tau_{3e}^{\mathrm{EB}})$, τ_{3e}^{M}, $C_{k\ 3\times1}^{M}(\tau_{3e}^{M})$, τ_{2e}^{C}, $C_{k\ 3\times1}^{C}(\tau_{2e}^{C})$, τ_{1e}^{EB}, $C_{k\ 3\times1}^{\mathrm{EB}}(\tau_{1e}^{\mathrm{EB}})$, τ_{1e}^{M} and $C_{k\ 3\times1}^{M}(\tau_{1e}^{M})$ when obtaining the barycenter positions of the central body and the Earth from the JPL ephemeris record.

2) Obtain light time solution of downlink and uplink radio signals as described in Moyer (2005), starting from t_{3s}. Then t_{2s} is computed iteratively, and, using this information t_{1s} is computed. Meanwhile, $\mathbf{X_E}(t_{3s})$, $\mathbf{X}_{\mathrm{GS}}(t_{3s})$, $\mathbf{X_C}(t_{2s})$, $\mathbf{X}_{\mathrm{SC}}(t_{2s})$, $\mathbf{X_E}(t_{1s})$ and $\mathbf{X}_{\mathrm{GS}}(t_{1s})$ are obtained. Moreover, we need to store values of τ_{3s}^{EB}, $C_{k\ 3\times1}^{\mathrm{EB}}(\tau_{3s}^{\mathrm{EB}})$, τ_{3s}^{M}, $C_{k\ 3\times1}^{M}(\tau_{3s}^{M})$, τ_{2s}^{C}, $C_{k\ 3\times1}^{C}(\tau_{2s}^{C})$, τ_{1s}^{EB}, $C_{k\ 3\times1}^{\mathrm{EB}}(\tau_{1s}^{\mathrm{EB}})$, τ_{1s}^{M} and $C_{k\ 3\times1}^{M}(\tau_{1s}^{M})$ when obtaining the barycenter positions of the central body and the Earth from JPL ephemeris record.
3) Compute $\mathbf{X}_{\mathrm{GS}}^{\mathbf{d}}$ and $\mathbf{X}_{\mathrm{GS}}^{\mathbf{u}}$ using Equation (8) and Equation (21) respectively.
4) If the central body is not the Sun, compute $\mathbf{X}_{\mathrm{SC}}$ using Equation (9). If the central body is the Sun, compute $\mathbf{X}_{\mathrm{SC}}$ using Equation (36).
5) Compute $\mathbf{X_E^d}$, $\mathbf{X_C}$ and $\mathbf{X_E^u}$ using Equations (25)–(27).
6) Compute $r_n^d(t_{3e}) - r_n^d(t_{3s})$ and $r_n^u(t_{3e}) - r_n^u(t_{3s})$ using Equation (2) and Equation (15) respectively.
7) Compute two-way Doppler observables using Equation (1).

It should be noted that the chosen order s in Equation (34) cannot be too large to ensure the computational efficiency. The best order is 3 or 4, which can balance both accuracy and efficiency.

2.4 Our updated Integrated Doppler Model (UID model)

The UTD model requires celestial ephemeris in the form of Chebyshev coefficients and polynomials and small counting intervals since the Taylor series needs to be convergent. However, if the celestial ephemeris is not in the form of Chebyshev coefficients and polynomials, such as for comet 67P, whose position and velocity are obtained by separate sliding-window Lagrange interpolation or the counting interval is larger, the UID model is a better choice.

As described in Andert (2010), the Doppler frequency shift for the downlink and uplink radio signal can be expressed as:

$$P_{\rm DL}(t_3) = 1 - \frac{f_{R_{\rm GS}}}{f_{T_{\rm SC}}} = 1 - \frac{1 - \mathrm{n}_{23}\beta_{\rm GS}(t_3) + \frac{1}{2}\|\beta_{\rm GS}(t_3)\|^2 - \frac{\phi_{\rm GS}(t_3)}{c^2_{\rm light}}}{1 - \mathrm{n}_{23}\beta_{\rm SC}(t_2) + \frac{1}{2}\|\beta_{\rm SC}(t_2)\|^2 - \frac{\phi_{\rm SC}(t_2)}{c^2_{\rm light}}} \tag{37}$$

$$P_{\rm UL}(t_3) = 1 - \frac{f_{R_{\rm SC}}}{f_{T_{\rm GS}}} = 1 - \frac{1 - \mathrm{n}_{12}\beta_{\rm SC}(t_2) + \frac{1}{2}\|\beta_{\rm SC}(t_2)\|^2 - \frac{\phi_{\rm SC}(t_2)}{c^2_{\rm light}}}{1 - \mathrm{n}_{12}\beta_{\rm GS}(t_1) + \frac{1}{2}\|\beta_{\rm GS}(t_1)\|^2 - \frac{\phi_{\rm GS}(t_1)}{c^2_{\rm light}}} \tag{38}$$

where t_3 is the midpoint of t_{3s} and t_{3e}, i.e. the time tag of two-day Doppler tracking data, t_1 is the transmission time corresponding to t_3, t_2 is the reflection time corresponding to t_3, n_{12} is the normalized vector from the ground station at time t_1 to the spacecraft at time t_2, n_{23} is the normalized vector from the spacecraft at time t_2 to the ground station at time t_3, and $\beta_{\rm GS}(t_1)$ and $\beta_{\rm GS}(t_3)$ are the normalized velocity of the ground station at time t_1 and t_3, respectively. $\beta_{\rm SC}(t_2)$ is the normalized velocity of the spacecraft at time t_2, and $\phi_{\rm GS}(t_1)$ and $\phi_{\rm GS}(t_3)$ are the gravity potential of the Sun and the planet in which the sphere of influence of the ground station is located at time t_1 and t_3, respectively. $\phi_{\rm SC}(t_2)$ is the gravity potential of the Sun and the planet in which the sphere of influence of the spacecraft is located at time t_2. $c_{\rm light}$ is the speed of light in a vacuum. The detailed formulas of n_{12}, n_{23}, $\beta_{\rm GS}(t_1)$, $\phi_{\rm GS}(t_1)$, $\beta_{\rm SC}(t_2)$, $\phi_{\rm SC}(t_2)$, $\beta_{\rm GS}(t_3)$ and $\phi_{\rm GS}(t_3)$ are described in Andert (2010).

In the UID model, Equation (37) and Equation (38) can be replaced by

$$P_{\rm DL}(t_3) = \frac{1}{T_c}\int_{t_{3s}}^{t_{3e}}\left(1 - \frac{f_{R_{\rm GS}}}{f_{T_{\rm SC}}}\right)dt \tag{39}$$

and

$$P_{\rm UL}(t_3) = \frac{1}{T_c}\int_{t_{3s}}^{t_{3e}}\left(1 - \frac{f_{R_{\rm SC}}}{f_{T_{\rm GS}}}\right)dt \tag{40}$$

respectively where T_c is the count time or count interval of the Doppler observables, $P_{\rm DL}(t_3)$ is the downlink Doppler effect and $P_{\rm UL}(t_3)$ is the uplink Doppler effect. $f_{R_{\rm GS}}$ is the frequency received by the ground station, $f_{T_{\rm SC}}$ is the frequency transmitted by the spacecraft, $f_{R_{\rm SC}}$ is the frequency received by the spacecraft and $f_{T_{\rm GS}}$ is the frequency transmitted by the ground station.

These two integrals over $[t_{3s},\ t_{3e}]$ can apply the n-node Gaussian quadrature rule and then result in the following approximations.

$$\int_{t_{3s}}^{t_{3e}}\left(1 - \frac{f_{R_{\rm GS}}}{f_{T_{\rm SC}}}\right)dt = \frac{(t_{3e} - t_{3s})}{2}\sum_{i=1}^{n} w_i P_{\rm DL}\left(\frac{t_{3e} - t_{3s}}{2}\xi_i + \frac{t_{3e} + t_{3s}}{2}\right) \tag{41}$$

and

$$\int_{t_{3s}}^{t_{3e}}\left(1 - \frac{f_{R_{\rm SC}}}{f_{T_{\rm GS}}}\right)dt = \frac{(t_{3e} - t_{3s})}{2}\sum_{i=1}^{n} w_i P_{\rm UL}\left(\frac{t_{3e} - t_{3s}}{2}\xi_i + \frac{t_{3e} + t_{3s}}{2}\right) \tag{42}$$

where w_i and ξ_i are coefficients for the n-node Gaussian quadrature rule. Finally, the two Doppler observables can be computed as

$$C_{\rm unramped} = c_{\rm light}\left(P_{\rm UL}(t_3) + P_{\rm DL}(t_3) - P_{\rm UL}(t_3)\,P_{\rm DL}(t_3)\right)\,. \tag{43}$$

3 MODEL VALIDATION AND ANALYSIS

The UTD and UID two-way Doppler models were implemented in the self-developed software tools WUDOGS (Jin et al. 2020). All the tests and analysis in this paper were performed by this software suite. It is noted that the differences between the different expressions for the relativistic Doppler effect are in the range of a few mHz (Andert 2010). The UTD and UID models are thus respectively validated since UTD model is the improved version of DRD model and UID model is the improved version of the model described in Andert (2010). In this section, these two models are respectively validated by two case studies of the Rosetta mission, which are the asteroid Lutetia flyby case and comet 67P

Table 5 The Mean Value (MV) and standard deviation (STD) of the Differences between Simulated Doppler Changes and Their Polynomial Fits Using UTD Model at Different Count Times

	1 s-count time		5 s-count time		10 s-count time	
$\mathrm{m\,s^{-1}}$	MV	STD	MV	STD	MV	STD
Equation (44)	1.1818e-07	6.8814e-04	1.1817e-07	1.3844e-04	1.1814e-07	6.8314e-05
Equation (45)	1.2091e-07	5.0376e-06	1.2091e-07	1.0244e-06	1.2090e-07	5.3174e-07

orbiting case. In these two cases, changes in the two-way Doppler observables due to the asteroid mass and comet 67P gravitational spherical harmonic coefficient C_{11} were respectively computed applying DRD and updated formulas. These changes were then fitted utilizing polynomials. The standard deviation of corresponding change residuals (the changes minus fit) reflects the numerical noise level. Similar methods for obtaining numerical noise level are presented in Zannoni & Tortora (2013), in which a "six-parameter fit" (Curkendal & McReynolds 1969) is used. However, "six-parameter fit" is a simple approach for determining the information content of Doppler data in heliocentric cruise instead of target flyby or orbiting phase (Curkendal & McReynolds 1969). Finally, numerical errors in the computation of the time in Chebyshev domain are discussed.

3.1 Case Study 1: Rosetta Asteroid Lutetia flyby—Validation and Analysis of UTD Model

Rosetta spacecraft performed a fly-by at asteroid Lutetia on 2010 July 10. During the flyby, the spacecraft was tracked with NASA's Deep Space Network (DSN) 70-m antenna (DSS 63) near Madrid, Spain and two-way Doppler tracking data were thus recorded at DSS 63 throughout the flyby (Pätzold et al. 2011). The numerical noise will be analyzed by computing the changes in the simulated two-way Doppler observables due to the mass of Lutetia. The simulation setup is summarized in Table 1.

Two sets of the simulated two-way Doppler observables can be generated by assuming a zero mass for Lutetia and by considering the Lutetia GM, respectively. Their difference is the Doppler change due to Lutetia GM. We compute this kind of "two-way Doppler" change with the DRD model, the GID model and the UTD model, as illustrated in Figure 2. The Doppler count intervals are chosen to be 1 s, 5 s and 10 s (upper, middle and lower in Fig. 2), respectively since the spacecraft passed by the asteroid rapidly.

In Figure 2, the blue lines mean the Doppler changes using different models. The red lines signify the polynomial fits for Doppler changes. The yellow lines indicate the residuals, which are the differences between the simulated Doppler changes and their polynomial fits. It can be seen that a number of numerical errors are introduced in the computation of "two-way Doppler difference" employing Moyer's DRD model. Also, the GID model was not effective for this case since the central body is the Sun. During the tracking span described in Table 1, the average Earth-spacecraft and Sun-spacecraft ranges are 3.05 AU and 2.72 AU respectively. Large numerical errors will be introduced if computing $\mathbf{X}_{\mathrm{SC}}$ utilizing Equation (9). However, we can see that curves related to the UTD model are smooth, indicating that the UTD model is less sensitive to numerical errors compared with the DRD model and the GID model. The mean value and standard deviation of the residuals (the differences between the simulated Doppler changes and their polynomial fits) are further computed, as summarized in Table 2.

During the Rosetta Lutetia flyby, the noise level of the two-way Doppler data recorded at DSS-63 at 1 s count time was around $0.1\,\mathrm{mm\,s^{-1}}$. Assuming a white phase noise, the noise level can be around $0.045\,\mathrm{mm\,s^{-1}}$ at 5 s count time and $0.032\,\mathrm{mm\,s^{-1}}$ at 10 s count time. We can see from the standard deviation that the accuracy of the computation of two-way Doppler observables relying on the DRD model and the traditional GID model are both close to the noise level of the measurement. Information on the mass of the asteroid is then obscured by the numerical noise. The UTD model, suggesting an accuracy of better than $6\times10^{-4}\,\mathrm{mm\,s^{-1}}$ at 10 s count time, shows a much better performance than the DRD and GID models.

3.2 Case Study 2: Rosetta comet 67P/Churyumov-Gerasimenko Orbiting—Validation and Analysis of the UID Model

When the Rosetta spacecraft began to escort the comet 67P in the autumn of 2014 (Godard et al. 2015), the center of integration changed into the comet. The ephemeris of comet 67P was generated by the Rosetta navigation group (Godard et al. 2015) and was then made into the form of SPICE SPK type-18 kernel (Acton 1996). The algorithms used by this type of kernel for the comet 67P implement separate sliding-window Lagrange interpolation of position and velocity instead of Chebyshev coefficients and polynomials. The UTD model cannot be thus used in the computation of two-way Doppler

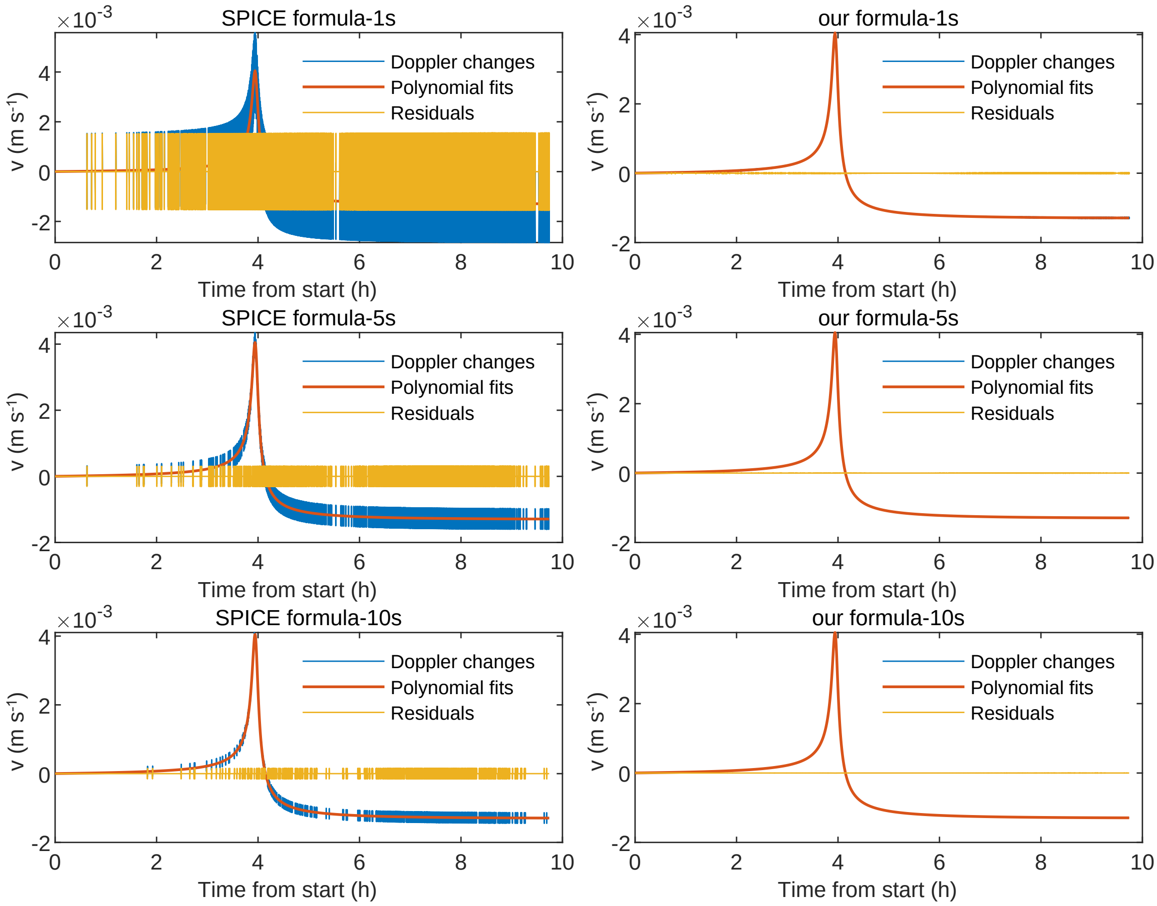

Fig. 4 Changes in simulated two-way Doppler observables due to the mass of Lutetia utilizing the UTD model at 1 s, 5 s and 10 s counting times, from top to bottom respectively.

observables in this case since the difference in barycenter position for the comet 67P at different time tags cannot be computed employing Equation (25). The UID model can then be chosen to reduce the numerical errors.

The way of validating and analyzing the UID model resembles those of case study 1. The changes in the simulated two-way Doppler observables due to C_{11} harmonic coefficient of the comet 67P gravity field are computed. Here we choose C_{11} because it is non-zero for comet 67P (Pätzold et al. 2016a) and the perturbation magnitude on Doppler observables is easy to be obscured by numerical noise. The simulation setups are described in Table 3. The orbital altitude during the chosen tracking pass is around 10 km.

Two sets of simulated two-way Doppler observables can be generated by assuming a zero C_{11} and by considering the given C_{11} harmonic coefficient, respectively. Their difference is the Doppler change due to the comet 67P C_{11} term. We compute this kind of "two-way Doppler" change with the DRD model and the UID model, as illustrated in Figure 3. The Doppler count intervals are chosen to be 10 s, 30 s and 60 s (upper, middle and lower in Fig. 3) respectively.

In Figure 3, the blue lines mean the Doppler changes using different models. The red lines signify the polynomial fits for Doppler changes utilizing different models. The yellow lines correspond to the residuals, which are the differences between the simulated Doppler changes and their polynomial fits. It can be seen that the change in the computed observables due to C_{11} harmonic coefficient is totally obscured by the numerical noise since the real shape of curves related to the DRD model cannot be shown. By contrast, the small numerical errors in the change due to C_{11} harmonic coefficient result in a smooth curve and a fit residual close to zero. Likewise, the mean value and standard deviation of the residuals (the differences between the simulated Doppler changes and their polynomial fits) are further computed, as summarized in Table 4.

The noise level of the two-way Doppler tracking data at 1 s count time is around 0.1 mm s^{-1}, resulting in the measurement accuracy at 10 s, 30 s and 60 s count time interval of around 0.032 mm s^{-1}, 0.018 mm s^{-1} and

$0.013\,\mathrm{mm\,s^{-1}}$, respectively. The standard deviations with DRD formulation are beneath but close to the measurement accuracy, suggesting an insufficient calculation accuracy. The UID model is by contrast marginally significant with respect to the measurement accuracy.

3.3 Numerical Errors Caused by the Time in Chebyshev Domain

In order to exploit the performance of both updated models, two details are necessary to stress here. One is the time representation in the navigation software, the other is the computation of time in the Chebyshev domain.

As described in Zannoni & Tortora (2013), the numerical noise is dominated by the time component, which reflects the range rate between the Earth station and the spacecraft. Our software thus represents the time using two variables in pairs (n_{tint}, t_{frac}), where n_{tint} is an integer, representing the number of Barycentric Dynamical Time (TDB) days that elapsed in J2000 and t_{frac} is a double precision value, representing the time in TDB seconds that elapsed since noon of the current day.

However, it is also necessary to discuss numerical errors in the computation of time in the Chebyshev domain. This factor exerts much influence on the UTD model but little influence on the UID model. This is because barycenter position differences of celestial bodies are computed in the UTD model, especially for the Earth. For some versions of celestial ephemeris such as the JPL ephemeris, corresponding official subroutines are provided for computing the time in Chebyshev domain to a high precision. However, official subroutines, related to some versions of celestial ephemeris such as the SPICE SPK kernel, are not accurate for computing the time in the Chebyshev domain.

The time tag of the SPICE SPK kernel is TDB seconds past the J2000.0 epoch. An SPK format planetary ephemeris contains one or more "segments," which contain Chebyshev polynomial coefficients for the position of the bodies as a function of time. One segment contains a number of records. The first two elements in each record are the midpoint and radius of the time interval covered by coefficients in this record. The other elements in the record are coefficients utilized for each component. The transformation, given in SPICE subroutines, from the domain of the record to the domain of Chebyshev polynomials (from –1 to 1), is computed as

$$\tau_{\mathrm{SPICE}} = \frac{t_{\mathrm{second}} - t_{\mathrm{mid}}}{t_{\mathrm{radius}}} \tag{44}$$

where τ_{SPICE} is the time in the domain of Chebyshev polynomials applying the formula given in SPICE subroutines, t_{mid} is the midpoint time in a single SPICE ephemeris record, t_{second} is the input time and t_{radius} is the length of a single SPICE ephemeris record. Here t_{second}, t_{mid} and t_{radius} are all TDB seconds past J2000. However, loss of significance will be also induced if time is represented by a single double-precision value, as described in Zannoni & Tortora (2013). An alternative formulation is expressed as

$$\tau_{\mathrm{SPICE}} = \frac{n_{\mathrm{tint}} - t_{\mathrm{mid}}}{t_{\mathrm{radius}}} + \frac{t_{\mathrm{frac}}}{t_{\mathrm{radius}}}\,. \tag{45}$$

Even though t_{mid} and t_{radius} are all TDB seconds past J2000, both of them are integer values or one integer value plus 1/2. No round-off errors will be induced for the representation of 1/2 using IEEE754 double-precision floating-point arithmetic. The first term in Equation (45) can be thus computed to a high precision. The second term will also not induce large numerical errors since t_{frac} is a small double-precision value.

The same steps with case study 1 are repeated here. Two sets of "two-way Doppler changes" due to Lutetia GM are computed utilizing the UTD model. The only difference is the choice of formulas for computation of Chebyshev time when computing $\mathbf{X}_{\mathbf{E}}^{\mathbf{d}}$ and $\mathbf{X}_{\mathbf{E}}^{\mathbf{u}}$. The count time interval is chosen to be 1 s, 5 s and 10 s.

In Figure 4, the blue lines mean the Doppler changes using different formulas for the time in Chebyshev domain. The red lines signify the polynomial fits for Doppler changes applying different formulas for the time in Chebyshev domain. The yellow lines correspond to the residuals, which are the differences between the simulated Doppler changes and their polynomial fits. It can be seen that large numerical errors are induced in the computation of the time in Chebyshev polynomial domain employing Equation (44), given in SPICE subroutines. The effect of numerical noise can be by contrast mitigated using Equation (45). The mean value and standard deviation of the residuals (the differences between the simulated Doppler changes and their polynomial fits) are summarized in Table 5. Equations (44) and (45) imply that Chebyshev time is computed utilizing Equation (44) and (45).

The numerical errors, as shown in Table 5, due to the computation of Chebyshev's time are larger than the measurement accuracy. The mass information of the target asteroid will be therefore obscured by numerical noise, which can be impaired using Equation (44). Of course, understanding the structure of different types of celestial ephemerides is the basis of utilizing Equation (45).

4 CONCLUSIONS

The traditional Moyer's DRD formulation is widely used for the computation of two-way Doppler observables. However, the computation of DRD formulation in the computer will induce a large loss of significance. This problem has been solved for some massive planet missions. However, few references discussed this problem for small body missions. In this paper, two updated models for small body missions, by the name of UTD model and UID model, were described in order to mitigate the effect of this type of numerical error. Both formulations and corresponding analysis were implemented in our own software suite—WUDOGS.

We first indicated that the main source of numerical noise in DRD formulation is the simple differencing between the geometrical range (first-order term) at the start of the counting interval and that at the end of the counting interval. The formulation and corresponding detailed instructions of the UTD model were then presented. This formulation, based upon the fact that the geometrical range difference can be expanded into a multidimensional Taylor series, is an improved version of GEODYN-II's interplanetary Doppler model. The most significant improvement is taking account of the case when the Sun is the center of integration. However, this formulation is merely effective for small count time. The UID formulation and corresponding detailed instructions were therefore presented for the case of larger count time. The two-way Doppler observables in this formulation are computed by the numerical integration of the Doppler frequency shift over the counting interval.

The UTD model and UID model were validated by two case studies of the Rosetta mission, which are the asteroid Lutetia flyby case and comet 67P orbiting case. The change in two-way Doppler observables due to asteroid Lutetia's mass was computed in the first case of asteroid Lutetia flyby. Large numerical errors due to the loss of significance were induced by the computation of Doppler observables applying the DRD model and GEODYN-II's interplanetary Doppler model. The magnitude of the errors is close to the measurement accuracy in actual practice of the mission whereas use of the UTD model can reduce the numerical noise in computed observables by two order-of-magnitude. Likewise, the change in two-way Doppler observables due to comet 67P's gravitational harmonic coefficient C_{11} were computed in the second case of comet 67P orbiting. The information on C_{11} in Doppler observables is totally obscured by large numerical errors induced by the DRD model whereas use of the UID model can also reduce the numerical noise in computed observables by two order-of-magnitude. Moreover, computing time in the Chebyshev domain, as one of the steps in UTD formulation, is also related to numerical errors caused by the loss of significance. Two formulations of computing the Chebyshev time were given at last for analyzing their contribution to numerical errors, as an example of Earth ephemeris of SPICE kernel.

In summary, numerical noise induced by the computation of two-way Doppler observables employing the DRD model is unneglectable. The noise level is very close to or even larger than the two-way Doppler measurement accuracy in the majority of current missions. UTD and UID formulation can be thus adopted since both of them showed an accuracy from better than 6×10^{-3} mm s^{-1} at 1 s counting time interval to better than 3×10^{-5} mm s^{-1} at 60 s counting time interval. The improvement indicated by the UTD and UID models will benefit spacecraft navigation of China's first asteroid exploration mission.

Acknowledgements This research is supported by the National Natural Science Foundation of China (Grant Nos. 42030110, 41874010 and U1831132) and Hubei Province Foundation innovation group project (2018CFA087). JPB was funded by a DAR grant in planetology from the French Space Agency (CNES). TA is funded by Deutsches Zentrum für Luft-und Raumfahrt, Bonn-Oberkassel (Grant Nos. 50QM1704 and 50QM1901).

Appendix A: DERIVATION OF UTD FORMULA

Basically, $r_n^d(t_{3s})$ and $r_n^d(t_{3e})$ can be expressed as:

$$r_n^d(t_{3s}) = \sqrt{\begin{array}{c}[(X_E(t_{3s}) + X_{\rm GS}(t_{3s})) - (X_C(t_{2s}) + X_{\rm SC}(t_{2s}))]^2 + \\ [(Y_E(t_{3s}) + Y_{\rm GS}(t_{3s})) - (Y_C(t_{2s}) + Y_{\rm SC}(t_{2s}))]^2 + \\ [(Z_E(t_{3s}) + Z_{\rm GS}(t_{3s})) - (Z_C(t_{2s}) + Z_{\rm SC}(t_{2s}))]^2\end{array}} \tag{A.1}$$

$$r_n^d(t_{3e}) = \sqrt{\begin{array}{c}[(X_E(t_{3e}) + X_{\rm GS}(t_{3e})) - (X_C(t_{2e}) + X_{\rm SC}(t_{2e}))]^2 + \\ [(Y_E(t_{3e}) + Y_{\rm GS}(t_{3e})) - (Y_C(t_{2e}) + Y_{\rm SC}(t_{2e}))]^2 + \\ [(Z_E(t_{3e}) + Z_{\rm GS}(t_{3e})) - (Z_C(t_{2e}) + Z_{\rm SC}(t_{2e}))]^2\end{array}} \tag{A.2}$$

$r_n^u(t_{3s})$ and $r_n^u(t_{3e})$ can be expressed as:

$$r_n^u(t_{3s}) = \sqrt{\begin{array}{c}[(X_E(t_{1s}) + X_{\rm GS}(t_{1s})) - (X_C(t_{2s}) + X_{\rm SC}(t_{2s}))]^2 + \\ [(Y_E(t_{1s}) + Y_{\rm GS}(t_{1s})) - (Y_C(t_{2s}) + Y_{\rm SC}(t_{2s}))]^2 + \\ [(Z_E(t_{1s}) + Z_{\rm GS}(t_{1s})) - (Z_C(t_{2s}) + Z_{\rm SC}(t_{2s}))]^2\end{array}} \tag{A.3}$$

$$r_n^u(t_{3e}) = \sqrt{\begin{array}{c}[(X_E(t_{1e}) + X_{\rm GS}(t_{1e})) - (X_C(t_{2e}) + X_{\rm SC}(t_{2e}))]^2 + \\ [(Y_E(t_{1e}) + Y_{\rm GS}(t_{1e})) - (Y_C(t_{2e}) + Y_{\rm SC}(t_{2e}))]^2 + \\ [(Z_E(t_{1e}) + Z_{\rm GS}(t_{1e})) - (Z_C(t_{2e}) + Z_{\rm SC}(t_{2e}))]^2\end{array}} \tag{A.4}$$

Let

$$X_E^d = X_E(t_{3e}) - X_E(t_{3s})$$
$$Y_E^d = Y_E(t_{3e}) - Y_E(t_{3s})$$
$$Z_E^d = Z_E(t_{3e}) - Z_E(t_{3s})$$
$$X_{\rm GS}^d = X_{\rm GS}(t_{3e}) - X_{\rm GS}(t_{3s})$$
$$Y_{\rm GS}^d = Y_{\rm GS}(t_{3e}) - Y_{\rm GS}(t_{3s})$$
$$Z_{\rm GS}^d = Z_{\rm GS}(t_{3e}) - Z_{\rm GS}(t_{3s})$$
$$X_C = X_C(t_{2e}) - X_C(t_{2s})$$
$$Y_C = Y_C(t_{2e}) - Y_C(t_{2s})$$

$$Z_C = Z_C(t_{2e}) - Z_C(t_{2s})$$
$$X_{\text{SC}} = X_{\text{SC}}(t_{2e}) - X_{\text{SC}}(t_{2s})$$
$$Y_{\text{SC}} = Y_{\text{SC}}(t_{2e}) - Y_{\text{SC}}(t_{2s})$$
$$Z_{\text{SC}} = Z_{\text{SC}}(t_{2e}) - Z_{\text{SC}}(t_{2s})$$
$$X_E^u = X_E(t_{1e}) - X_E(t_{1s})$$
$$Y_E^u = Y_E(t_{1e}) - Y_E(t_{1s})$$
$$Z_E^u = Z_E(t_{1e}) - Z_E(t_{1s})$$
$$X_{\text{GS}}^u = X_{\text{GS}}(t_{1e}) - X_{\text{GS}}(t_{1s})$$
$$Y_{\text{GS}}^u = Y_{\text{GS}}(t_{1e}) - Y_{\text{GS}}(t_{1s})$$
$$Z_{\text{GS}}^u = Z_{\text{GS}}(t_{1e}) - Z_{\text{GS}}(t_{1s}) \tag{A.5}$$

The $r_n^d(t_{3e})$ and $r_n^u(t_{3e})$ can be expressed as:

$$r_n^d(t_{3e}) = \sqrt{\begin{gathered}\left[\left(X_E(t_{3s}) + X_E^d + X_{\text{GS}}(t_{3s}) + X_{\text{GS}}^d\right) - \left(X_C(t_{2s}) + X_C + X_{\text{SC}}(t_{2s}) + X_{\text{SC}}\right)\right]^2 + \\ \left[\left(Y_E(t_{3s}) + Y_E^d + Y_{\text{GS}}(t_{3s}) + Y_{\text{GS}}^d\right) - \left(Y_C(t_{2s}) + Y_C + Y_{\text{SC}}(t_{2s}) + Y_{\text{SC}}\right)\right]^2 + \\ \left[\left(Z_E(t_{3s}) + Z_E^d + Z_{\text{GS}}(t_{3s}) + Z_{\text{GS}}^d\right) - \left(Z_C(t_{2s}) + Z_C + Z_{\text{SC}}(t_{2s}) + Z_{\text{SC}}\right)\right]^2\end{gathered}} \tag{A.6}$$

$$r_n^u(t_{3e}) = \sqrt{\begin{gathered}\left[\left(X_E(t_{1s}) + X_E^u + X_{\text{GS}}(t_{1s}) + X_{\text{GS}}^u\right) - \left(X_C(t_{2s}) + X_C + X_{\text{SC}}(t_{2s}) + X_{\text{SC}}\right)\right]^2 + \\ \left[\left(Y_E(t_{1s}) + Y_E^u + Y_{\text{GS}}(t_{1s}) + Y_{\text{GS}}^u\right) - \left(Y_C(t_{2s}) + Y_C + Y_{\text{SC}}(t_{2s}) + Y_{\text{SC}}\right)\right]^2 + \\ \left[\left(Z_E(t_{1s}) + Z_E^u + Z_{\text{GS}}(t_{1s}) + Z_{\text{GS}}^u\right) - \left(Z_C(t_{2s}) + Z_C + Z_{\text{SC}}(t_{2s}) + Z_{\text{SC}}\right)\right]^2\end{gathered}} \tag{A.7}$$

Then, we obtain

$$r_n^d(t_{3e}) = \sqrt{\begin{gathered}\left(r_n^d(t_{3s})\right)^2 + \\ 2\left(X_E(t_{3s}) + X_{\text{GS}}(t_{3s}) - X_C(t_{2s}) - X_{\text{SC}}(t_{2s})\right)\left(X_E^d + X_{\text{GS}}^d - X_C - X_{\text{SC}}\right) + \\ 2\left(Y_E(t_{3s}) + Y_{\text{GS}}(t_{3s}) - Y_C(t_{2s}) - Y_{\text{SC}}(t_{2s})\right)\left(Y_E^d + Y_{\text{GS}}^d - Y_C - Y_{\text{SC}}\right) + \\ 2\left(Z_E(t_{3s}) + Z_{\text{GS}}(t_{3s}) - Z_C(t_{2s}) - Z_{\text{SC}}(t_{2s})\right)\left(Z_E^d + Z_{\text{GS}}^d - Z_C - Z_{\text{SC}}\right) + \\ \left(X_E^d + X_{\text{GS}}^d - X_C - X_{\text{SC}}\right)^2 + \\ \left(Y_E^d + Y_{\text{GS}}^d - Y_C - Y_{\text{SC}}\right)^2 + \\ \left(Z_E^d + Z_{\text{GS}}^d - Z_C - Z_{\text{SC}}\right)^2\end{gathered}} \tag{A.8}$$

$$r_n^u(t_{3e}) = \sqrt{\begin{gathered}\left(r_n^d(t_{1s})\right)^2 + \\ 2\left(X_E(t_{1s}) + X_{\text{GS}}(t_{1s}) - X_C(t_{2s}) - X_{\text{SC}}(t_{2s})\right)\left(X_E^u + X_{\text{GS}}^u - X_C - X_{\text{SC}}\right) + \\ 2\left(Y_E(t_{1s}) + Y_{\text{GS}}(t_{1s}) - Y_C(t_{2s}) - Y_{\text{SC}}(t_{2s})\right)\left(Y_E^u + Y_{\text{GS}}^u - Y_C - Y_{\text{SC}}\right) + \\ 2\left(Z_E(t_{1s}) + Z_{\text{GS}}(t_{1s}) - Z_C(t_{2s}) - Z_{\text{SC}}(t_{2s})\right)\left(Z_E^u + Z_{\text{GS}}^u - Z_C - Z_{\text{SC}}\right) + \\ \left(X_E^u + X_{\text{GS}}^u - X_C - X_{\text{SC}}\right)^2 + \\ \left(Y_E^u + Y_{\text{GS}}^u - Y_C - Y_{\text{SC}}\right)^2 + \\ \left(Z_E^u + Z_{\text{GS}}^u - Z_C - Z_{\text{SC}}\right)^2\end{gathered}} \tag{A.9}$$

In order to simplify the formula, we use the following substitutions,

$$X^u = X_E^u + X_{\text{GS}}^u - X_C - X_{\text{SC}}$$
$$Y^u = Y_E^u + Y_{\text{GS}}^u - Y_C - Y_{\text{SC}}$$
$$Z^u = Z_E^u + Z_{\text{GS}}^u - Z_C - Z_{\text{SC}}$$
$$X^d = X_E^d + X_{\text{GS}}^d - X_C - X_{\text{SC}}$$
$$Y^d = Y_E^d + Y_{\text{GS}}^d - Y_C - Y_{\text{SC}}$$
$$Z^d = Z_E^d + Z_{\text{GS}}^d - Z_C - Z_{\text{SC}}$$
$$R_x^u = X_E(t_{1s}) + X_{\text{GS}}(t_{1s}) - X_C(t_{2s}) - X_{\text{SC}}(t_{2s})$$
$$R_y^u = Y_E(t_{1s}) + Y_{\text{GS}}(t_{1s}) - Y_C(t_{2s}) - Y_{\text{SC}}(t_{2s})$$
$$R_z^u = Z_E(t_{1s}) + Z_{\text{GS}}(t_{1s}) - Z_C(t_{2s}) - Z_{\text{SC}}(t_{2s})$$

$$
\begin{aligned}
R_x^d &= X_E\left(t_{3s}\right) + X_{\text{GS}}\left(t_{3s}\right) - X_C\left(t_{2s}\right) - X_{\text{SC}}\left(t_{2s}\right)\\
R_y^d &= Y_E\left(t_{3s}\right) + Y_{\text{GS}}\left(t_{3s}\right) - Y_C\left(t_{2s}\right) - Y_{\text{SC}}\left(t_{2s}\right)\\
R_z^d &= Z_E\left(t_{3s}\right) + Z_{\text{GS}}\left(t_{3s}\right) - Z_C\left(t_{2s}\right) - Z_{\text{SC}}\left(t_{2s}\right)
\end{aligned}
\tag{A.10}
$$

Then, the $r_n^d\left(t_{3e}\right)$ and $r_n^u\left(t_{3e}\right)$ at time t_{3e} become a function of (X^d, Y^d, Z^d) and (X^u, Y^u, Z^u), respectively:

$$
\begin{aligned}
r_n^d\left(t_{3e}\right) &= f_d\left(X^d, Y^d, Z^d\right)\\
&= \sqrt{\left(r_n^d\left(t_{3s}\right)\right)^2 + 2R_x^d X^d + 2R_y^d Y^d + 2R_z^d Z^d + \left(X^d\right)^2 + \left(Y^d\right)^2 + \left(Z^d\right)^2}
\end{aligned}
\tag{A.11}
$$

$$
\begin{aligned}
r_n^u\left(t_{3e}\right) &= f_u\left(X^u, Y^u, Z^u\right)\\
&= \sqrt{\left(r_n^u\left(t_{3s}\right)\right)^2 + 2R_x^u X^u + 2R_y^u Y^u + 2R_z^u Z^u + \left(X^u\right)^2 + \left(Y^u\right)^2 + \left(Z^u\right)^2}
\end{aligned}
\tag{A.12}
$$

Furthermore, $\left(X^d, Y^d, Z^d\right)$ can be treated as the downlink change vector $\mathbf{D}$, whose corresponding unit vector is $\mathbf{n_d}$. (X^u, Y^u, Z^u) can be treated as the uplink change vector $\mathbf{U}$, whose corresponding unit vector is $\mathbf{n_u}$. R_x^d, R_y^d and R_z^d can be regarded as the three components of the vector $\mathbf{R_d}$, and R_x^u, R_y^u and R_z^u can be regarded as the three components of the vector $\mathbf{R_u}$. When the count time is small, $r_n^d\left(t_{3e}\right)$ can be written as a Taylor series that is calculated from the values of the derivatives of f_d at (0,0,0).

$$
\begin{aligned}
r_n^d\left(t_{3e}\right) - r_n^d\left(t_{3s}\right) =& f_d^{(1)}\left(0,0,0\right)\|\mathbf{D}\| + \frac{1}{2}f_d^{(2)}\left(0,0,0\right)\|\mathbf{D}\|^2 +\\
&\frac{1}{6}f_d^{(3)}\left(0,0,0\right)\|\mathbf{D}\|^3 + O\left(\|\mathbf{D}\|^3\right)
\end{aligned}
\tag{A.13}
$$

where the derivatives are

$$
f_d^{(1)}\left(0,0,0\right) = \frac{\mathbf{n_d}\mathbf{R_d}}{r_n^d\left(t_{3s}\right)}
\tag{A.14}
$$

$$
f_d^{(2)}\left(0,0,0\right) = \frac{r_n^d\left(t_{3s}\right) - \frac{1}{r_n^d\left(t_{3s}\right)}\left(\mathbf{n_d}\mathbf{R_d}\right)}{\left(r_n^d\left(t_{3s}\right)\right)^2}
\tag{A.15}
$$

$$
f_d^{(3)}\left(0,0,0\right) = \frac{-3r_n^d\left(t_{3s}\right)\left(\mathbf{n_d}\mathbf{R_d}\right) + \frac{3}{r_n^d\left(t_{3s}\right)}\left(\mathbf{n_d}\mathbf{R_d}\right)^3}{\left(r_n^d\left(t_{3s}\right)\right)^4}
\tag{A.16}
$$

Likewise,

$$
\begin{aligned}
r_n^u\left(t_{3e}\right) - r_n^u\left(t_{3s}\right) =& f_u^{(1)}\left(0,0,0\right)\|\mathbf{U}\| + \frac{1}{2}f_u^{(2)}\left(0,0,0\right)\|\mathbf{U}\|^2 +\\
&\frac{1}{6}f_u^{(3)}\left(0,0,0\right)\|\mathbf{U}\|^3 + O\left(\|\mathbf{U}\|^3\right)
\end{aligned}
\tag{A.17}
$$

where the derivatives are

$$
f_u^{(1)}\left(0,0,0\right) = \frac{\mathbf{n_u}\mathbf{R_u}}{r_n^u\left(t_{3s}\right)}
\tag{A.18}
$$

$$
f_u^{(2)}\left(0,0,0\right) = \frac{r_n^u\left(t_{3s}\right) - \frac{1}{r_n^u\left(t_{3s}\right)}\left(\mathbf{n_u}\mathbf{R_u}\right)}{\left(r_n^u\left(t_{3s}\right)\right)^2}
\tag{A.19}
$$

$$
f_u^{(3)}\left(0,0,0\right) = \frac{-3r_n^u\left(t_{3s}\right)\left(\mathbf{n_u}\mathbf{R_u}\right) + \frac{3}{r_n^u\left(t_{3s}\right)}\left(\mathbf{n_u}\mathbf{R_u}\right)^3}{\left(r_n^u\left(t_{3s}\right)\right)^4}
\tag{A.20}
$$

Finally, $(X_{\text{GS}}^d, Y_{\text{GS}}^d, Z_{\text{GS}}^d)$ and $(X_{\text{GS}}^u, Y_{\text{GS}}^u, Z_{\text{GS}}^u)$ can be calculated directly by Equation (A.10). $(X_{\text{SC}}, Y_{\text{SC}}, Z_{\text{SC}})$ is calculated by Equation (41). (X_E^u, Y_E^u, Z_E^u), (X_E^d, Y_E^d, Z_E^d) and (X_C, Y_C, Z_C) should be computed using the Chebyshev polynomial differencing scheme. Here we give the following derivation of the scheme in Appendix B.

Appendix B: DERIVATION OF BARYCENTER CELESTIAL POSITION DIFFERENCE AT TWO DIFFERENT EPOCHS

Two different epochs are named t_a and t_b. Here we assume that t_b is larger than t_a. Basically, the position of a celestial body at time t_t $\mathbf{X_R}(t_t)$ can be calculated by the following expansion

$$
\mathbf{X_R}\left(t_t\right) = \sum_{k=0}^{N-1} C_{k3\times1}\left(\tau_t\right).P_k\left(\tau_t\right)
\tag{B.1}
$$

$P_k(\tau_t)$ is computed utilizing the recurrence relationship

$$\begin{gathered} P_0(\tau_t) = 0 \\ P_1(\tau_t) = \tau \\ \ldots \\ P_k(\tau_t) = 2\tau_t P_{k-1}(\tau_t) - P_{k-2}(\tau_t) \end{gathered} \tag{B.2}$$

where τ_t is time t_t normalized between –1 and +1 on the time interval covered by the coefficients. The change in body position from time t_a to time t_b can be computed as

$$\mathbf{X_R} = \sum_{k=0}^{N-1} \left[C_{k3\times1}(\tau_b) P_k(\tau_b) - C_{k3\times1}(\tau_a) P_k(\tau_a)\right] \tag{B.3}$$

Suppose that

$$\begin{cases} C_{k_{3\times1}} = C_{k3\times1}(\tau_b) - C_{k3\times1}(\tau_a) \\ P_k = P_k(\tau_b) - P_k(\tau_a) \end{cases} \tag{B.4}$$

$\mathbf{X_R}$ can be rewritten as

$$\mathbf{X_R} = \sum_{k=0}^{N-1} \left[C_{k3\times1}(\tau_a) P_k + C_{k_{3\times1}} P_k(\tau_b)\right] \tag{B.5}$$

where P_k is computed relying on the following recurrence relationship.

$$\begin{gathered} P_0 = 0 \\ P_1 = \tau_b - \tau_a \\ \ldots \\ P_k = 2\tau_b P_{k-1} + 2(\tau_b - \tau_a) P_k(\tau_a) - P_{k-2} \end{gathered} \tag{B.6}$$

The position of the Earth is obtained from the position of the Earth-Moon barycenter and the Earth's Moon. This scheme for the Earth is therefore computed as Equation (26) and Equation (27).

References

Acton, C. H. 1996, Planet. Space Sci., 44, 65

Andert, T. P. 2010, Masses of Small Bodies: Mass Estimation of Small Solar System Bodies Using Radio Science Data from Close Flybys, PhD Thesis, Universitätsbibliothek

Armstrong, J. W., Iess, L., Tortora, P., & Bertotti, B. 2003, ApJ, 599, 806

Centinello, Frank J., I., Zuber, M. T., Smith, D. E., & Mazarico, E. 2015, Journal of Spacecraft and Rockets, 52, 1331

Curkendal, D. W., & McReynolds, S. R. 1969, Journal of Spacecraft and Rockets, 6, 520

Folkner, W. M., Williams, J. G., Boggs, D. H., Park, R. S., & Kuchynka, P. 2014, Interplanetary Network Progress Report, 42-196, 1

Godard, B., Budnik, F., Muñoz, P., Morley, T., & Janarthanan, V. 2015, in Proceedings 25th International Symposium on Space Flight Dynamics–25th ISSFD, Munich, Germany

IEEE. 2019, Institute of Electrical and Electronics Engineers New York

Iess, L., Di Benedetto, M., Marabucci, M., & Racioppa, P. 2012, in 23rd International Symposium on Space Flight Dynamics

Jin, W. T., Li, F., Yan, J. G., et al. 2020, MNRAS, 493, 4012

Montenbruck, O., & Gill, E. 2012, Satellite Orbits: Models, Methods and Applications (Springer Science & Business Media)

Moyer, T. D. 1971, Mathematical Formulation of the Double-Precision Orbit Determination Program (DPODP). (California Inst. Technology, Pasadena, California. Techn. Report 32-1527)

Moyer, T. D. 2005, Formulation for Observed and Computed Values of Deep Space Network Data Types for Navigation, 3 (John Wiley & Sons)

Pätzold, M., Wennmacher, A., Häusler, B., et al. 2001, A&A, 370, 1122

Pätzold, M., Andert, T. P., Asmar, S. W., et al. 2011, Science, 334, 491

Pätzold, M., Andert, T., Hahn, M., et al. 2016a, Nature, 530, 63

Pätzold, M., Häusler, B., Tyler, G. L., et al. 2016b, Planet. Space Sci., 127, 44

Rowlands, D., Marshall, J., McCarthy, J., et al. 2015, Hughes-STX Contractor Report, https://space-geodesy.nasa.gov/techniques/tools/GEODYN/geodyn_vol1.pdf

Tommei, G., Milani, A., & Vokrouhlický, D. 2010, Celestial Mechanics and Dynamical Astronomy, 107, 285

Zannoni, M., & Tortora, P. 2013, Journal of Guidance Control Dynamics, 36, 1008